Preliminary Assessment of Precast Reinforced Concrete Columns against Close-in Air Blast

Swee Hong TAN, Hui Qi LOH and Jiing Koon POON
Ministry of Home Affairs, Singapore

Abstract

In this contribution, a series of initial numerical results with respect to structural response of precast reinforced concrete (RC) columns subjected to close-in air blast are discussed. Although it is widely established that precast components generally possess limited blast resilience due to their non-monolithic connections, the underlying mechanisms are not well understood. To this end, the present study seeks to gain further insights via explicit modelling of a typical grouted sleeve connection, involving the bond behavior along reinforcement laps and the contacts between interacting concrete surfaces at the column base.

Eurocodes have replaced British Standards as Singapore's prescribed building codes for structural design since 2015. CEB-FIP Model Code 1990 has served as an important basis for Eurocode 2: Design of Concrete Structures. In absence of experimental data, this study adopts the relevant guidance from the revised fib Model Code 2010, in attempt to incorporate the latest recommendations numerically. Two key departures are observed vis-à-vis the 1990 version. First, the fracture energy, which characterizes the tensile softening phenomenon, is now solely a function of mean unconfined compressive strength, i.e. independent of maximum aggregate size, while second, the local bond stress-slip analytical model that predicts the interaction between reinforcing bar and concrete, has largely remained the same, albeit with different input parameters.

1. Introduction

In late 2017, the Construction Industry Transformation Map was implemented to promote productivity and to reduce reliance on foreign labour in Singapore (1). It calls for industry adoption of Design for Manufacturing & Assembly (DfMA), which broadly refers to the modular design of building components for efficient and clean site installation, as well as the highly automated offsite production facilities. In the same year, an updated Code of Buildability was released to legislate the minimum Buildable Design scores required of new developments and the mandatory use of specific productive technologies as part of Government Land Sale (GLS) Programme (2).

Precast reinforced concrete (RC) construction, which falls within the DfMA framework, is naturally an option for consideration by local structural engineers to fulfil prevailing statutory requirements. While the design and assessment procedures for precast RC elements are well established with respect to conventional buildings, the contrary holds true for atypical loading condition such as blast effects.

Traditionally, blast-resistant components are cast-in-situ with the necessary flexural and diagonal tension reinforcement to offer sufficient inbound and rebound resistances against air blast. Precast RC elements are only recommended for large standoff distances (> 2 kg/m$^{1/3}$) if the connections are adequately designed to handle support reactions during both inbound and rebound responses (3). Broadly, the detailing rules are similar to those during seismic design, i.e. continuity of flexural bars, especially at the areas where plasticity is expected, as well as the use of closed spaced ties and links throughout the span of component (4, 5).

Furthermore, Singapore is located in a low-seismicity region and only designs of selected structures founded on certain ground types are required to address tremors due to distant earthquakes (6-8). As a result, majority of precast RC structures do not have moment-resisting connections, as opposed to a seismic framing system whereby beam-column continuity is critical to ensure global structural response against strong lateral forces. Conventional precast RC system in Singapore typically involves beams supported by corbels to take gravity loadings, in tandem with shear walls located within staircases and lift-cores for lateral loadings (9-11), as shown in Figure 1.

Against this backdrop, the Ministry of Home Affairs in Singapore has plans to conduct full-scale blast trials, in support of the development of a generalized design framework for precast RC columns subjected to close-in air blast. In this contribution, a series of initial numerical results with respect to structural response of precast RC columns subjected to close-in air blast are discussed. Current study builds upon the knowledge gathered from past in-house work on the modelling of RC components using LS-DYNA® (12-16).

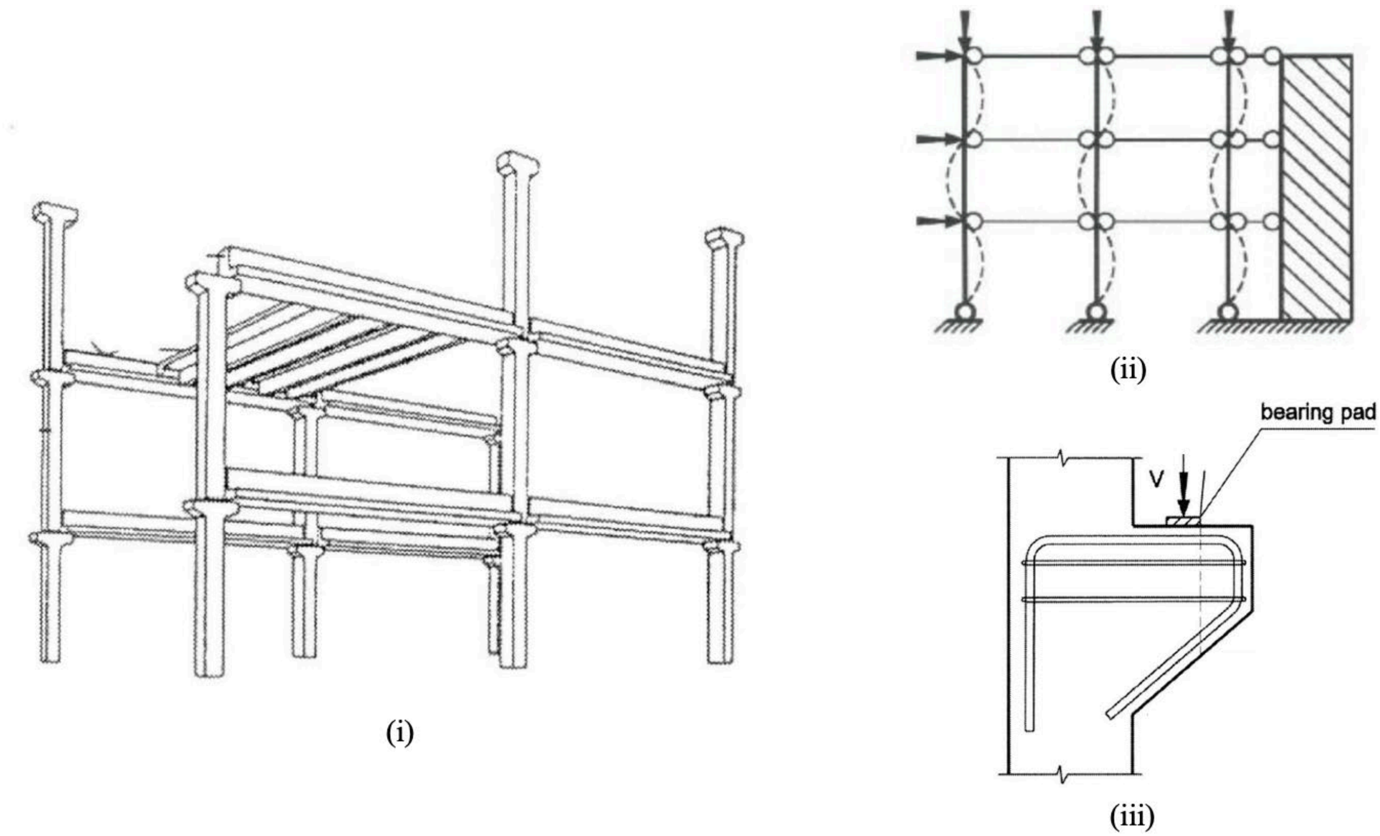

Figure 1: (i) Typical precast RC system involving beams supported on corbels to take gravity loadings; (ii) Schematics of a lateral-resisting configuration for a precast RC system; and (iii) Close-up view of a beam-column connection, whereby the precast RC beam transfers shear reaction onto a corbel via a bearing pad.

2. Objective of Work

The present study seeks to gain insights about the behavior of precast RC columns subjected to close-in air blast at scaled distances lesser than the recommended range of 2 kg/m$^{1/3}$ given in the prevailing design methodology (3). At the same time, the study aims to establish broad performance benchmarks, below which retrofits to the precast RC columns are necessary to mitigate against significant loss in axial load-carrying capacity. This series of initial numerical work is meant to offer first-cut evaluation of the problem in hand. Further detailed analyses will be carried out to achieve a comprehensive understanding towards pre-test planning for the full-scale blast trials. The ultimate objective is to develop a generalized design framework for practical applications in Singapore.

3. Idealization of Precast RC Column

To this end, preliminary calculations are first carried out to establish meaningful structural configurations for the numerical analyses. In accordance to prevailing Eurocodes (17, 18) and Singapore National Annexes (19, 20), a lower bound dimension for a square precast RC column to serve imposed loads under Category E (Industrial Use) is derived to be 600 mm based on an equivalent stress formulation (21), assuming 8 m-by-8 m bay in a 5-storey structure. The flexural reinforcement is next computed by stipulating a tensile reinforcement ratio of approximately 1%, so that the ensuing section remains under-reinforced as part of standard good practice for blast-resistant design to prevent sudden compression failure (5). This is then followed by the estimation of the required diagonal tension reinforcement to satisfy the ultimate inbound and rebound resistances (3), assuming fixed-fixed (top and bottom) boundary conditions over a span of 4500 mm.

The characteristic compressive cylinder strength of concrete at 28 days is taken to be 35 MPa while the secant modulus of elasticity of concrete is 34 GPa, as given in Table 3.1 of SS EN 1992-1-1 (18). The characteristic yield strength of reinforcement is taken to be 500 MPa with the relevant strength and deformation properties of steel as per Grade B500C (22), following a classical elastic-plastic strain hardening profile without rate effects.

The precast RC column is adjoined to its base support using a typical grouted sleeve connection. At this region, the flexural reinforcement within the precast RC column is lapped with the starter bars protruding from the base support, as illustrated in Figure 2. The concrete cover to the nearest flexural reinforcement is maintained at 75 mm throughout the span of column, as shown in Figure 3. This accounts for the presence of the corrugated pipes of 50 mm diameter (through which the starter bars are emplaced before grouting), as well as the surrounding diagonal tension reinforcement which offer confinement to the flexural bars. The corrugated pipes are not modeled explicitly in this study for simplicity, in avoidance of high computational costs. Instead, attention has been given to two other physical phenomena which are postulated to have greater influence on the response of the precast RC column against close-in air blast. They are namely (i) the bond of embedded flexural reinforcement, and (ii) the contacts between interacting concrete surfaces at the base of precast RC column.

In view that the previous CEB-FIP Model Code 1990 is an important technical basis for SS EN 1992-1-1, extensive reference has been made to the latest fib Model Code 2010 (23), in order to numerically characterize the two physical phenomena. In this study, two local bond-slip relationships in the Table 6.1-1 of fib Model Code 2010 are investigated, i.e. pull-out and splitting (stirrups), both under good bond conditions. The static coefficient of friction is taken as 0.6 with respect to a smooth interface as per Section 6.3.3 of fib Model Code 2010, while its dynamic counterpart is assumed to be 0.3. In this study, mesh size of 20 mm is kept consistent as far as possible for all concrete (constant stress) solid elements and steel (Hughes-Liu with cross section integration) beam elements. Mesh refinement has not been considered. It will be carried out as part of future work.

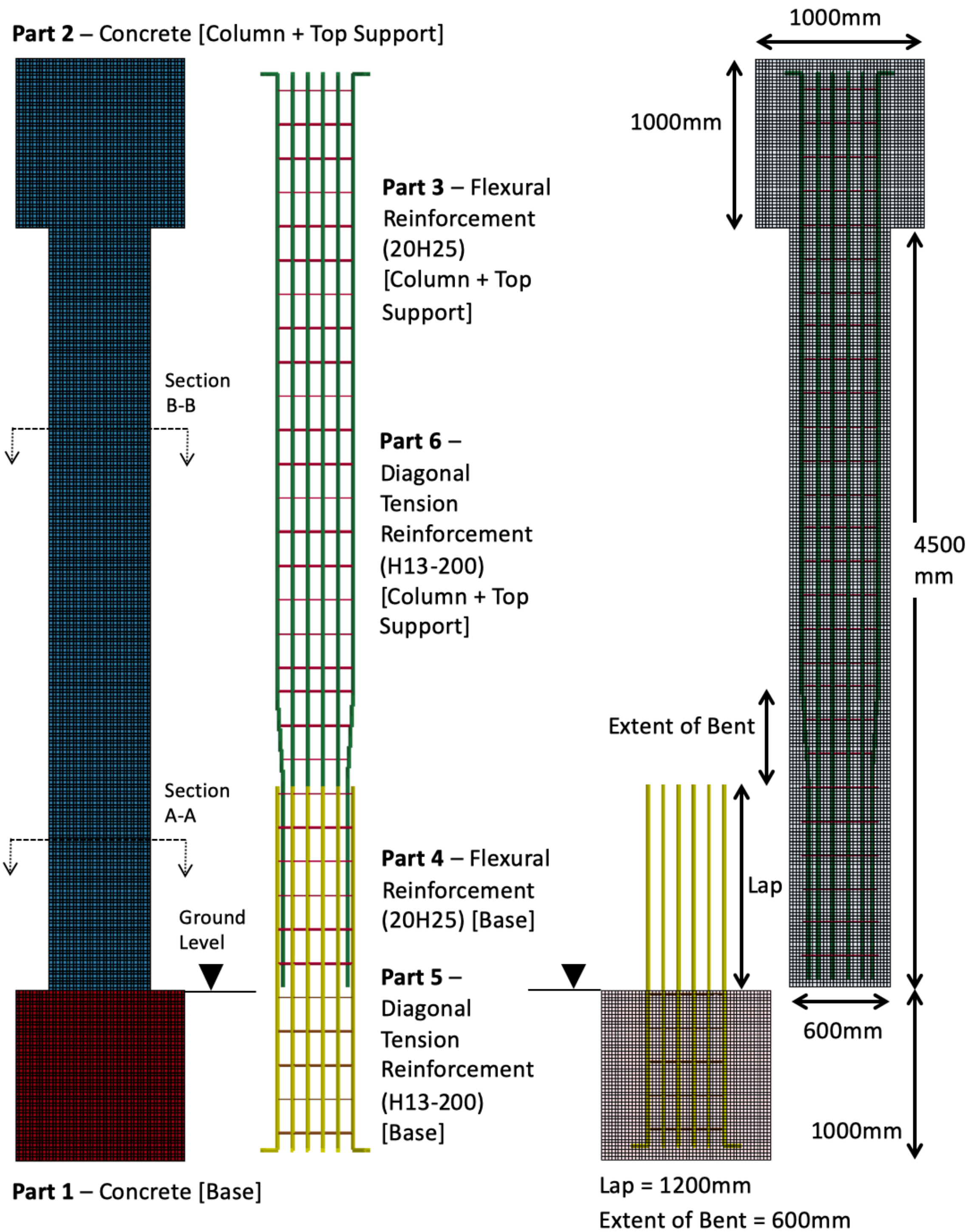

(i) (ii)

Figure 2: (i) Idealization of a precast RC column involving various concrete and reinforcement parts; and (ii) Illustration on how the precast RC column is adjoined to its base support, while its flexural reinforcement laps with the starter bars protruding from the base support.

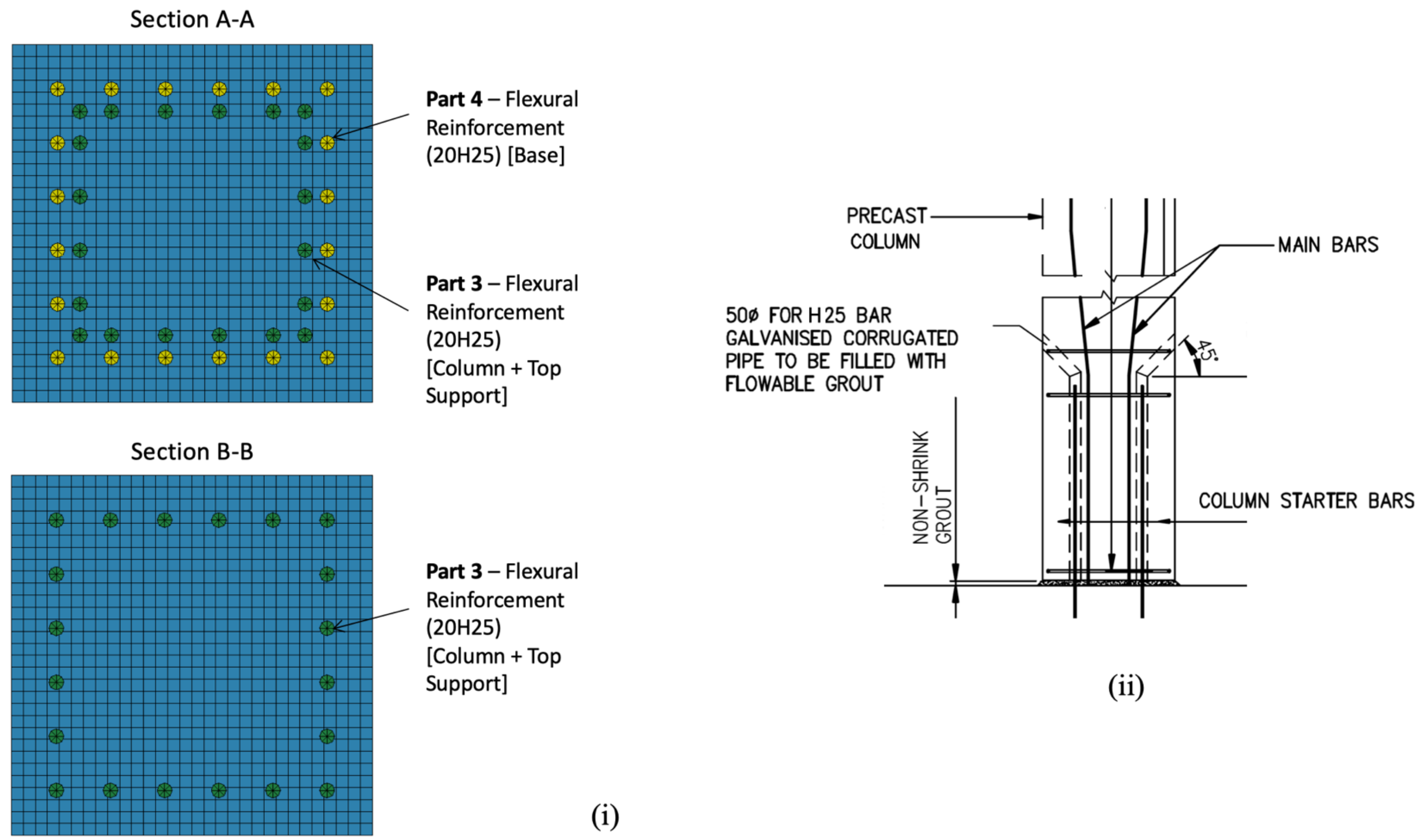

Figure 3: (i) Section views of the arrangement of flexural reinforcement within the idealized precast RC column; and (ii) Schematics of a typical grouted sleeve connection between a precast RC column and its base support.

4. Parametric Numerical Analyses

This study involves a series of parametric numerical analyses. The underlying motivation is to determine the varying responses arising from different modelling assumptions and considerations, and to identify knowledge gaps for detailed follow-up investigation as part of future work. A total of five parameters are accounted for.

First, up to five threat scenarios consisting of various combinations of charge weight and scaled distances are analyzed. For confidentiality purposes, the two charge weights used are denoted as $4\boldsymbol{x}$ and $\boldsymbol{x}$ respectively. Hemispherical surface burst is assumed at scaled distances of 0.4 kg/m$^{1/3}$, 0.6 kg/m$^{1/3}$ and 0.8 kg/m$^{1/3}$, in order to stay within the applicability of the empirical equations underlying the air blast characteristics, as well as to be significantly lower than the minimum criteria of 2 kg/m$^{1/3}$ set by prevailing design methodology (3).

Second, two concrete material models, namely *MAT_CDPM (24) and *MAT_RHT (25), are employed extensively. The bilinear damage formulation within *MAT_CDPM is characterized to reflect the latest guidance regarding the fracture energy, which is now solely a function of mean unconfined compressive strength of 43 MPa as per Table 3.1 of SS EN 1992-1-1, i.e. independent of maximum aggregate size, in the latest fib Model Code 2010. The strain rate flag in *MAT_CDPM is turned off as a conservative measure, on account that inertia effects can already be captured at high strain rate for compression (26), albeit not as well under tension due to localization (27). The erosion flag in *MAT_CDPM is also turned off, although it is later observed that element deletion continues to occur unexpectedly whenever full restart is implemented. Similar to *MAT_CDPM, the auto-generation function of *MAT_RHT is exercised, except that the shear modulus is amended to correlate with the secant modulus of elasticity of concrete of 34 GPa and Poisson's Ratio of 0.2 for uncracked concrete (18). The strain rate dependence in *MAT_RHT is maintained. Material model *MAT_72R3 is considered initially (28). It is subsequently dropped from parametric studies, due to observations that severe element distortion can happen, even at relatively large scaled distances. The cause can be attributed to its inherently low fracture energy.

A series of uniaxial tensile test on a single 20 mm element with varying parameter b_2 reveals that the default cracking characteristics within *MAT_72R3 are hardcoded and cannot be modified to represent a user-defined fracture energy. Parameter locwidth has been set to a value lesser than 20 mm to effect localization within the single element. Further comparison between single element simulations involving all three concrete material models confirms that *MAT_CDPM is able to recover the desired fracture energy of 0.144 N/mm based on mean unconfined compressive strength of 43 MPa, while *MAT_72R3 continues to benchmark its cracking characteristics against the previous CEB-FIP Model Code 1990 (27), as shown in Figure 4. For *MAT_RHT, the strain rate effects cannot be deactivated readily, and therefore the single element simulation must be conducted with prescribed nodal displacements applied over prolonged duration in order to retrieve a near quasi-static behavior. Even so, there is still some enhancement observed above the peak tensile stress which should rightfully be 3.2 MPa, following Table 3.1 of SS EN 1992-1-1. Overall, the fracture energy generated automatically by *MAT_RHT clearly surpasses the other two material models. The material cards for all three concrete models, as well as that for reinforcement (*MAT_PIECEWISE_LINEAR_PLASTICITY), is given in the Appendix.

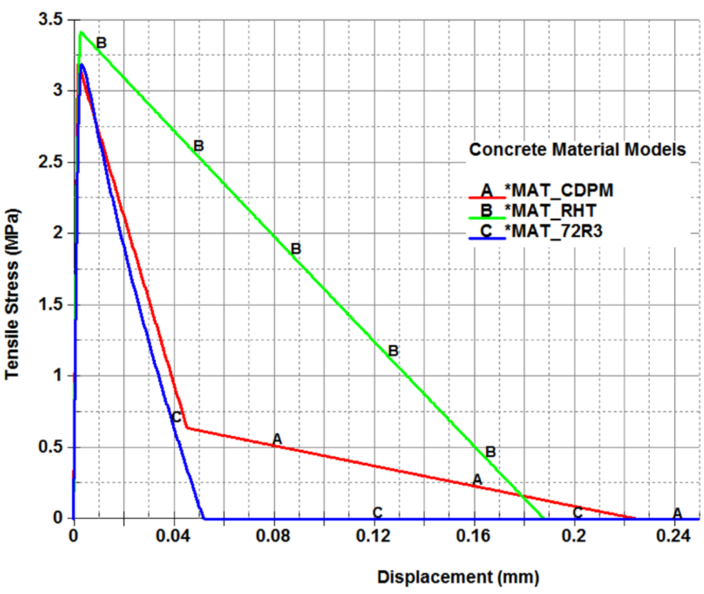

(i)

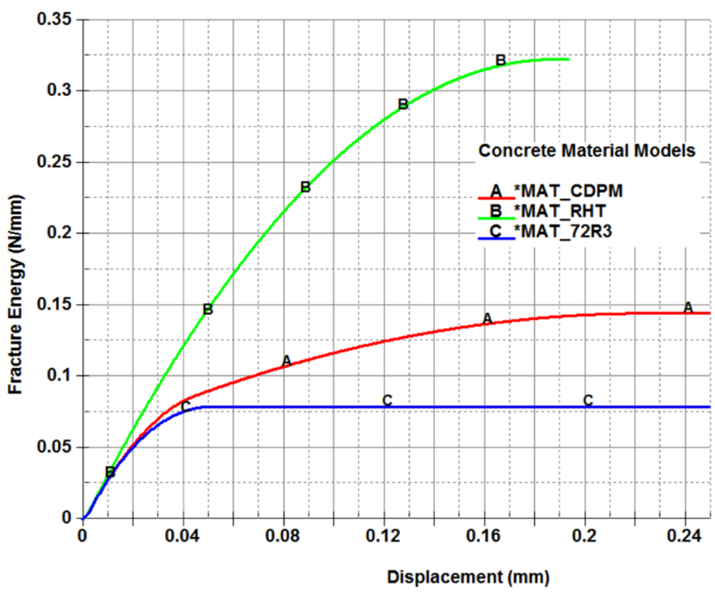

(ii)

Figure 4: Uniaxial tensile test on a single 20 mm element involving *MAT_CDPM, *MAT_RHT and *MAT_72R3. (i) Graph of tensile stress against prescribed nodal displacements; and (ii) Graph of fracture energy against prescribed nodal displacements.

Third, two sets of (top and bottom) boundary conditions are explored, namely fixed-fixed and guided-fixed. These boundary conditions are implemented by imposing the appropriate translational nodal constraints to the base and top support, as illustrated in Figure 2. The reason for doing so is to determine the likely bounds of responses of the precast RC column against close-in air blast. Recall that, majority of precast RC structures in Singapore do not have moment-resisting connections and the gravity load-resisting beams are inherently weak as they do not possess sufficient inbound and rebound resistances. Therefore, fixed-fixed boundary conditions represent a situation whereby the connecting beam at the floor level is not severely damaged and continues to offer lateral restraint to the top of column against the direction of blast (e.g. perimeter columns with minimal blast leakage through the building envelope), while the contrary is true for guided-fixed boundary conditions (e.g. interior columns with the beams exposed to direct blast effects). The former requires full translational nodal constraints in all directions, while the latter does the same except for the top support in the direction of blast.

Fourth, two axial preloads, namely 3000 kN and 7500 kN, are included. Physically, an axial preload represents a pre-blast stress state induced by a tributary combination of structural self-weight, as well as superimposed dead loads and live loads applied on every floor of the building. In order to establish a practical range of pre-blast stress states, the axial load that correlates with the maximum moment capacity in a typical column interaction diagram, as well as the maximum axial capacity (in absence of bending) are first determined (21).

The nominal balanced axial load and full axial capacity are computed to be approximately 5000 kN and 16000 kN respectively for the column shown in Figure 2. Therefore, the value of 3000 kN is chosen to capture behavior at around 20% of maximum capacity (16000 kN), in recognition that it is the minimum benchmark beyond which members are identified under combined compression and flexure and are subjected to more conservative limits on the allowable flexural response during typical blast-resistant design (3). On the other hand, the value of 7500 kN is selected to tally with 150% of balanced load (5000 kN) as a reasonable upper bound of service load within the compression-controlled zone. In lieu of dynamic relaxation (29), transient explicit method is employed to achieve the pre-blast stress states. Prior estimation of the column's natural period is necessary. Prescribed nodal displacements are invoked over a long duration of at least 15 times of the natural period to obtain a near quasi-static state of response. Two runs are required to recover each axial preload exactly; analytical approximation of the column deformation, followed by adjustment of the correlating prescribed nodal displacements.

Fifth, three cases of axial coupling using *CONSTRAINED_BEAM_IN_SOLID are considered. Case 1 involves full-directional constraints to the acceleration and velocity of the embedded flexural reinforcement in concrete by setting the keyword parameter CDIR to null. Case 2 and 3 consider coupling only in the normal direction and releases the axial constraints, such that the axial coupling force can be computed as a user-defined function of slip between the rebar nodes and the concrete solid elements, i.e. CDIR equals 1. As mentioned earlier, two local bond-slip relationships in the Table 6.1-1 of fib Model Code 2010 are investigated; Case 2 – pull-out, while Case 3 - splitting (stirrups), under good bond conditions with reference to definitions in SS EN 1992-1-1. The card inputs for both user-defined functions are provided in the Appendix.

5. Numerical Results

Finally, the findings from this series of parametric studies are discussed. In total, up to 120 idealized precast RC column models are investigated. They collectively represent various combinations of the five parameters highlighted in the preceding section. For ease of reference, the mean quantities arising from the three cases of axial coupling are presented, together with the maximum coefficient of variation across each threat scenario.

In order to assess the applicability of under-integrated solid elements, the ratio between the hourglass and internal energies are first tabulated, as shown in Table 1. The most onerous Scenario 1 results in numerical instability near the bottom of the column, leading to non-physical solutions, for both concrete material models as shown in Figure

5. Although it appears that *MAT_CDPM has out-performed *MAT_RHT with lesser extent of zero-energy deformation modes, it has happened at the expense of erosion. Notwithstanding that element deletion continues to occur despite its inactive flag, its presence already cast some doubts on the admissibility of the results.

For such complex problems, the hourglass energy should ideally be lesser than ±10% of the internal energy. Therefore, if a benchmark is drawn based on results from *MAT_RHT, only the related findings from Scenario 4 and 5 for both concrete material models are strictly acceptable. Nevertheless, since this is a preliminary assessment with mesh refinement yet to be carried out, all idealized precast RC column models with the exception of Scenario 1, are further subjected to post-blast simulations to ascertain the residual axial capacities.

Table 1: Mean ratio between hourglass energy and internal energy, computed based on the three cases of axial coupling, with the respective maximum coefficient of variation across each threat scenario; (i) *MAT_CDPM; and (ii) *MAT_RHT.

(i) ***MAT_CDPM**

			Ratio between Hourglass Energy and Internal Energy				
			Mean [%]				
			Fixed-Fixed BCs		Guided-Fixed BCs		
Scenario No.	Charge Weight	Scaled Distance [kg/m$^{1/3}$]	P_0 = 3000kN	P_0 = 7500kN	P_0 = 3000kN	P_0 = 7500kN	Maximum Coefficient of Variation [%]
1	$4x$	0.4	Numerical instability, leading to non-physical solution. See example in Figure 5(i).				Not Applicable
2	x	0.4	2.23	2.20	2.20	2.27	7.61
3	$4x$	0.6	2.90	2.57	3.43	3.18	14.34
4	x	0.6	2.57	1.53	2.43	1.59	15.37
5	$4x$	0.8	1.83	1.03	1.80	1.00	16.45

(ii) ***MAT_RHT**

			Ratio between Hourglass Energy and Internal Energy				
			Mean [%]				
			Fixed-Fixed BCs		Guided-Fixed BCs		
Scenario No.	Charge Weight	Scaled Distance [kg/m$^{1/3}$]	P_0 = 3000kN	P_0 = 7500kN	P_0 = 3000kN	P_0 = 7500kN	Maximum Coefficient of Variation [%]
1	$4x$	0.4	Numerical instability, leading to non-physical solution. See example in Figure 5(ii).				Not Applicable
2	x	0.4	19.70	15.47	19.97	15.98	8.08
3	$4x$	0.6	22.03	18.20	24.00	20.70	4.93
4	x	0.6	11.07	7.67	10.03	8.90	12.62
5	$4x$	0.8	9.97	7.73	8.80	6.79	13.12

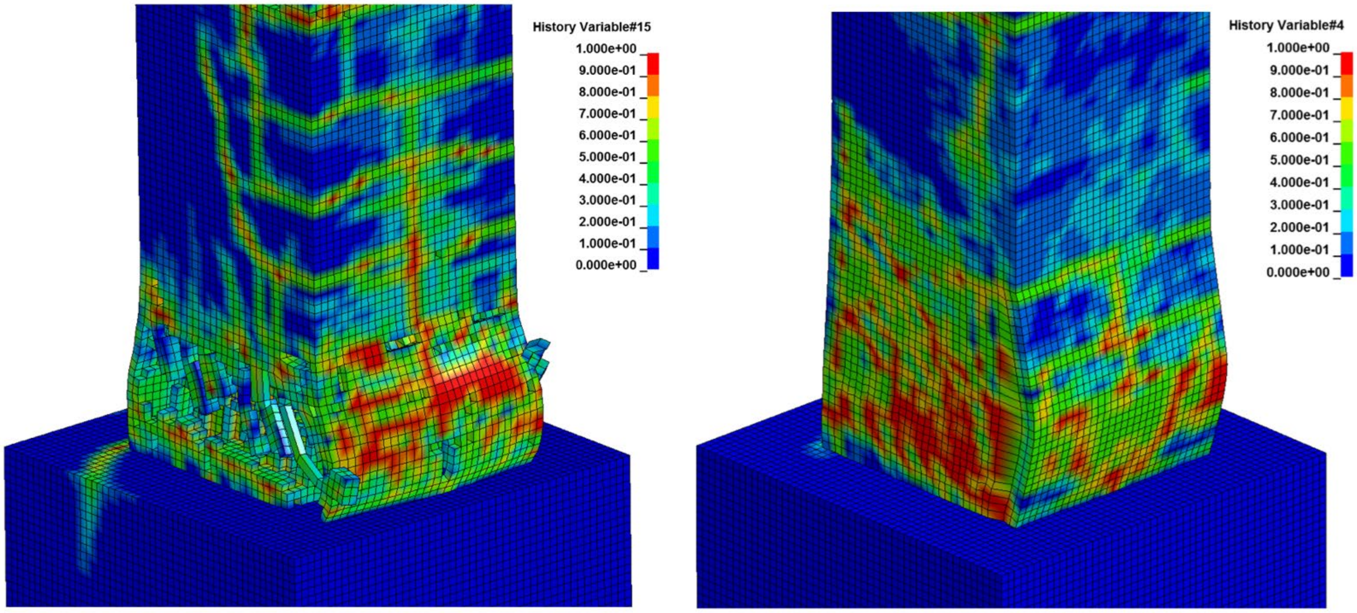

(i) (ii)

Figure 5: Examples of numerical instability, leading to non-physical solutions for Scenario 1 involving *MAT_CDPM and *MAT_RHT. (i) Plot of tensile damage variable via History Variable 15 for *MAT_CDPM; and (ii) Plot of damage parameter via History Variable 4 for *MAT_RHT.

The prediction of the peak displacements by the various models are next summarized, as given in Table 2. The locations at which the peak displacements occur, depart expectedly between the two sets of (top and bottom) boundary conditions. For fixed-fixed boundary conditions, the maximum response is captured at the mid-span while for guided-fixed, near the top of column. There is negligible difference between the peak displacements computed using the three cases of axial coupling, as seen from the relatively small percentages of maximum coefficient of variation per threat scenario. However, in terms of the order of magnitude, the peak displacements generated under guided-fixed boundary conditions exceed that under fixed-fixed due to lower lateral stiffnesses. Ceteris paribus, the axial preloads are not found to have significant influence on the peak displacements.

The post-blast residual axial capacities are lastly compiled. The predictions are given as percentages of the maximum axial capacities in Table 3, which are computed by subjecting pristine precast RC column models under prescribed nodal displacements to the top support till failure. Three observations can be made. First, both maximum axial capacities obtained numerically are higher than that using the semi-analytical formulation (16000 kN) (21), ranging from 15% to 25% increase against *MAT_CDPM and *MAT_RHT respectively. This is anticipated, in view of the structural imperfections and other miscellaneous experimental factors underlying the code approach. Second, higher axial preload generally improves the residual performance for all models, except for those in Scenario 3. Notwithstanding earlier remark on its admissibility due to either extensive erosion or zero-energy deformation modes, this correlates with another observation that Scenario 3 has accounted for the largest set of peak displacements as compared to the remaining threat scenarios for both concrete material models in Table 2. One reasonable explanation is that the detrimental effects arising from a higher axial preload coupled with greater deformation, have outweighed the enhancement to the overall shear resistance. Recall that, it is conservative to ignore the presence of compression on the shear strength of concrete in typical blast-resistant design (3). Third, the choice of axial coupling has negligible impact on the ensuing residual axial capacities.

Table 2: Mean peak displacements, computed based on the three cases of axial coupling, with the respective maximum coefficient of variation across each threat scenario; (i) *MAT_CDPM; and (ii) *MAT_RHT.

(i) ***MAT_CDPM**

Scenario No.	Charge Weight	Scaled Distance [kg/m$^{1/3}$]	Peak Displacement [mm] – Mean [mm] – Fixed-Fixed BCs: P_0 = 3000kN	Fixed-Fixed BCs: P_0 = 7500kN	Guided-Fixed BCs: P_0 = 3000kN	Guided-Fixed BCs: P_0 = 7500kN	Maximum Coefficient of Variation [%]
1	4x	0.4	Numerical instability, leading to non-physical solution. See example in Figure 5(i).				Not Applicable
2	x	0.4	9.39	8.21	12.33	12.97	2.91
3	4x	0.6	18.03	17.13	34.67	40.10	2.07
4	x	0.6	6.30	5.62	8.90	8.84	1.15
5	4x	0.8	11.77	10.60	22.53	22.57	0.42

(ii) ***MAT_RHT**

Scenario No.	Charge Weight	Scaled Distance [kg/m$^{1/3}$]	Peak Displacement [mm] – Mean [mm] – Fixed-Fixed BCs: P_0 = 3000kN	Fixed-Fixed BCs: P_0 = 7500kN	Guided-Fixed BCs: P_0 = 3000kN	Guided-Fixed BCs: P_0 = 7500kN	Maximum Coefficient of Variation [%]
1	4x	0.4	Numerical instability, leading to non-physical solution. See example in Figure 5(ii).				Not Applicable
2	x	0.4	10.53	10.00	21.23	21.37	1.10
3	4x	0.6	18.63	20.07	55.60	58.70	4.59
4	x	0.6	6.15	5.93	9.90	9.50	1.00
5	4x	0.8	11.00	11.90	24.60	28.00	7.83

6. Conclusion

The ultimate objective is to develop a generalized design framework for practical applications in Singapore. The numerical results obtained so far are preliminary. Efforts are required to resolve the knowledge gaps which have been identified along the way. At this juncture, one scope which warrants dedicated attention, is the inability to enact user-defined softening characteristics of *MAT_72R3 in tension. Fracture energy appears to be a key limiting factor in the performance of precast RC columns subjected to close-in air blast. The non-monolithic grouted sleeve connection at the bottom of the column receives high pressure loads due to its close proximity to the source of detonation. Severe stress wave concentrations aggravated by the discontinuity in concrete, further contributes to extensive tensile failure near the bottom of the column, as shown in Figure 6. Future work shall also entail physical variations in column dimensions, tensile reinforcement ratio and grade of steel reinforcement, as well as other numerical aspects regarding additional concrete material models, damping, material strain rate effects and mesh refinement. Retrofit options using steel collars at the base of the column will also be explored.

Table 3: Mean ratio between residual axial capacity and maximum axial capacity, computed based on the three cases of axial coupling, with the respective maximum coefficient of variation across each threat scenario; (i) *MAT_CDPM; and (ii) *MAT_RHT.

(i) ***MAT_CDPM**

Scenario No.	Charge Weight	Scaled Distance [kg/m$^{1/3}$]	Ratio between Residual Axial Capacity and Maximum Axial Capacity – Mean [%] – Fixed-Fixed BCs		Guided-Fixed BCs		Maximum Coefficient of Variation [%]
			P_0 = 3000kN	P_0 = 7500kN	P_0 = 3000kN	P_0 = 7500kN	
1	$4x$	0.4	Numerical instability, leading to non-physical solution. See example in Figure 5(i).				Not Applicable
2	x	0.4	88	92	88	91	6.65
3	$4x$	0.6	65	59	57	42	6.86
4	x	0.6	91	92	94	95	0.27
5	$4x$	0.8	79	83	93	93	2.13

Maximum Axial Capacity 18297 kN

(ii) ***MAT_RHT**

Scenario No.	Charge Weight	Scaled Distance [kg/m$^{1/3}$]	Ratio between Residual Axial Capacity and Maximum Axial Capacity – Mean [%] – Fixed-Fixed BCs		Guided-Fixed BCs		Maximum Coefficient of Variation [%]
			P_0 = 3000kN	P_0 = 7500kN	P_0 = 3000kN	P_0 = 7500kN	
1	$4x$	0.4	Numerical instability, leading to non-physical solution. See example in Figure 5(ii).				Not Applicable
2	x	0.4	*	92	*	89	*
3	$4x$	0.6	85	70	67	52	8.52
4	x	0.6	93	95	97	97	0.51
5	$4x$	0.8	87	92	91	92	2.38

Maximum Axial Capacity 20477 kN

Note:

* Not completed in time for the submission of the manuscript.

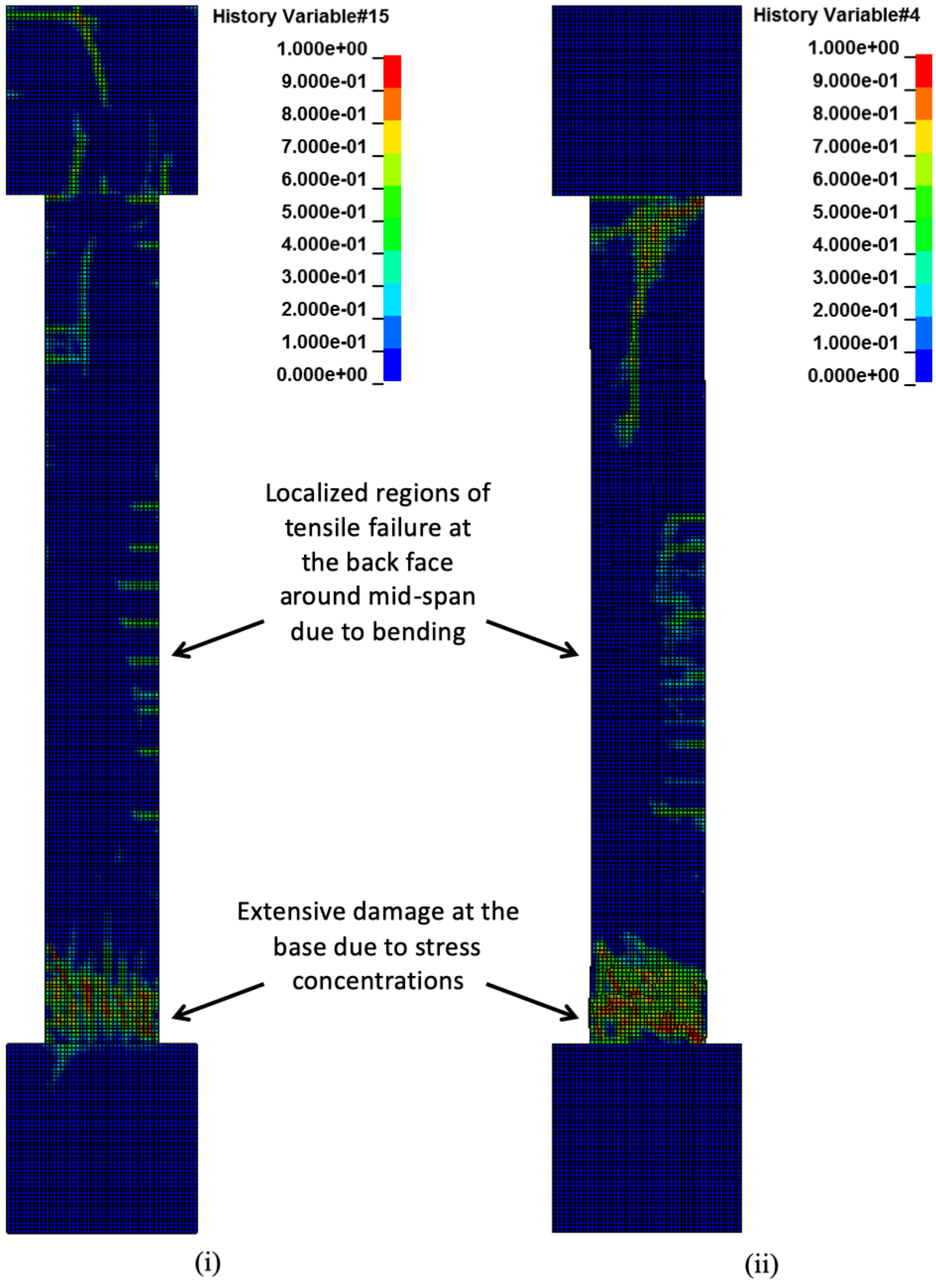

Figure 6: Examples of post-blast column damage profiles for scenarios involving *MAT_CDPM and *MAT_RHT. (i) Plot of tensile damage variable via History Variable 15 for *MAT_CDPM with respect to Scenario 2 – Guided-Fixed BCs – P_0 = 7500 kN; and (ii) Plot of damage parameter via History Variable 4 for *MAT_RHT with respect to Scenario 3 – Fixed-Fixed BCs – P_0 = 3000 kN.

Appendix

Material Cards

Concrete

```
*MAT_CDPM
$---+----1----+----2----+----3----+----4----+----5----+----6----+----7----+----8
$        |         |         |         |         |         |         |         |
$      MID       RHO         E        PR       ECC       QH0        FT        FC
         1   2.3E-03     34000       0.2                             3.2        35
$        |         |         |         |         |         |         |         |
$       HP        AH        BH        CH        DH        AS        DF       FC0
     0.001
$        |         |         |         |         |         |         |         |
$     TYPE        BS        WF       WF1       FT1    STRFLG   FAILFLG       EFC
         1         1  0.224469  0.044894      0.64         0         0      1e-4


*MAT_RHT
$#     mid        ro     shear   onempa      epsf        b0        b1        t1
         1   2.3E-03     14167 -5.000000  2.000000     0.000     0.000     0.000
$#       a         n        fc       fs*       ft*        q0         b        t2
     0.000     0.000     0.000     0.000   0.09143     0.000     0.000     0.000
$#     e0c       e0t        ec        et     betac     betat       ptf
     0.000     0.000     0.000     0.000     0.000     0.000  0.001000
$#     gc*       gt*        xi        d1        d2       epm        af        nf
     0.000     0.000     0.000     0.000     0.000     0.000     0.000     0.000
$#   gamma        a1        a2        a3       pel       pco        np     alpha
     0.000     0.000     0.000     0.000     0.000     0.000     0.000     0.000


*MAT_Concrete_Damage_Rel3
$    MATID        RO        PR
         1 2.300E-03 2.000E-01
$       ft        A0        A1        A2        B1     OMEGA       A1F
 3.200E+00 1.035E+01 4.463E-01 2.309E-03 1.058E+00 5.000E-01 4.417E-01
$  sLambda      NOUT     EDROP     RSIZE       UCF    LCRate  LocWidth      NPTS
 1.000E+02 2.000E+00 1.000E+00 3.972E-02 1.450E+02 0.000E+00 6.000E+01 1.300E+01
$ Lambda01  Lambda02  Lambda03  Lambda04  Lambda05  Lambda06  Lambda07  Lambda08
 0.000E+00 8.000E-06 2.400E-05 4.000E-05 5.600E-05 7.200E-05 8.800E-05 3.200E-04
$ Lambda09  Lambda10  Lambda11  Lambda12  Lambda13        B3       A0Y       A1Y
 5.200E-04 5.700E-04 1.000E+00 1.000E+01 1.000E+10 1.150E+00 7.812E+00 6.250E-01
$    Eta01     Eta02     Eta03     Eta04     Eta05     Eta06     Eta07     Eta08
 0.000E+00 8.500E-01 9.700E-01 9.900E-01 1.000E+00 9.900E-01 9.700E-01 5.000E-01
$    Eta09     Eta10     Eta11    Eta012     Eta13        B2       A2F       A2Y
 1.000E-01 0.000E+00 0.000E+00 0.000E+00 0.000E+00 1.350E+00 3.380E-03 7.357E-03
```

Reinforcement

```
*MAT_PIECEWISE_LINEAR_PLASTICITY_TITLE
500MPa Reinforcement
$#     mid        ro         e        pr      sigy      etan      fail      tdel
         2  0.007850 2.0000E+5  0.300000       500      1724    0.0725     0.000
$#       c         p      lcss      lcsr        vp
     0.000     0.000         0         0         0
$#    eps1      eps2      eps3      eps4      eps5      eps6      eps7      eps8
     0.000     0.000     0.000     0.000     0.000     0.000     0.000     0.000
$#     es1       es2       es3       es4       es5       es6       es7       es8
     0.000     0.000     0.000     0.000     0.000     0.000     0.000     0.000
```

<u>*User-Defined Functions*</u>

*Axial Coupling via *CONSTRAINED_BEAM_IN_SOLID*

Case 2 (Pull-out – Good Bond Condition)

```
*DEFINE_FUNCTION
$# Local bond stress-slip relationship
$# fib Model Code 2010 Table 6.1-1 Column 1;
$# Pull-out (PO) - Good Bond Condition
$#     fid
        25
float force(float slip,float leng)
{float force,pi,d,area,shear,tmax,tfinal,s1,s2,s3,alpha;
pi = 3.141592654;
d = 25;
area = pi*d*leng;
tmax = 16.3936;
tfinal = 0.4*tmax;
s1 = 1;
s2 = 2;
s3 = 0.5*d;
alpha = 0.4;
if (slip < s1) {shear = tmax*(slip**alpha);}
else if (slip < s2) {shear = tmax;}
else if (slip < s3) {shear = tmax - (slip - s2)/(s3 - s2)*(tmax - tfinal);}
else {shear = tfinal;}
force = shear*area;
return force;}
```

Case 3 (Splitting (SP) – Stirrups – Good Bond Condition)

```
*DEFINE_FUNCTION
$# Local bond stress-slip relationship
$# fib Model Code 2010 Table 6.1-1 Column 4;
$# Splitting (SP) - Stirrups - Good Bond Condition
$#     fid
        25
float force(float slip,float leng)
{float force,pi,d,area,shear,tmax,tsplit,tfinal,s1,s2,s3,alpha;
pi = 3.141592654;
d = 25;
area = pi*d*leng;
tmax = 16.3936;
tsplit = 9.1616;
tfinal = 0.4*tsplit;
s1 = 0.2335;
s2 = 1;
s3 = 0.5*d;
alpha = 0.4;
if (slip < s1) {shear = tmax*(slip**alpha);}
else if (slip < s2) {shear = tsplit;}
else if (slip < s3) {shear = tsplit - (slip - s2)/(s3 - s2)*(tsplit - tfinal);}
else {shear = tfinal;}
force = shear*area;
return force;}
```

References

1. Building and Construction Authority (BCA) S. BCA BuildSG Construction Industry Transformation Map [Available from: https://www1.bca.gov.sg/buildsg/construction-industry-transformation-map-ITM.
2. Code of Practice on Buildability (2017 Edition): Building and Construction Authority (BCA), Singapore; 2017.
3. PDC TR-06-01 Rev. 1 Single Degree of Freedom Blast Design Spreadsheets (SBEDS) Methodology. US Department of Defense (DOD); 2008.
4. ASCE/SEI 59-11: Blast Protection of Buildings. American Society of Civil Engineers (ASCE); 2011.
5. UFC 3-340-02: Structures to Resist The Effects of Accidental Explosions, With Change 2 (1 September 2014). US Department of Defense (DOD); 2014.
6. SS EN 1998-1: 2013 Eurocode 8: Design of structures for earthquake resistance - Part 1: General rules, seismic actions and rules for buildings. Enterprise Singapore; 2013.
7. NA SS EN 1998-1: 2013 Singapore National Annex to Eurocode 8: Design of structures for earthquake resistance - Part 1: General rules, seismic actions and rules for buildings. Enterprise Singapore; 2013.
8. BC3: 2013 Guidebook for Design of Buildings in Singapore to Requirements in SS EN 1998-1: Building and Construction Authority (BCA), Singapore; 2013.
9. Design for Manufacturing and Assembly (DfMA) - Connections for Advanced Precast Concrete System: Building and Construction Authority (BCA), Singapore; 2018.
10. Structural Precast Concrete Handbook. 2nd ed: Building and Construction Authority (BCA), Singapore; 2001.
11. Bulletin 43 - Structural connections for precast concrete buildings. International Federation for Structural Concrete (fib); 2008.
12. Poon JK, Tay SK, Chan R, Schwer L. Simulating Dynamic Loads on Concrete Components using the MM-ALE (Eulerian) Solver. 11th European LS-DYNA Conference: DYNAmore GmbH; 2017.
13. Tan SH, Chan R, Poon JK, Chng D. Verification of Concrete Material Models for MM-ALE Simulations. 13th International LS-DYNA Users Conference: Livermore Software Technology Corporation; 2014.
14. Tan SH, Poon JK, Chan R, Chng D. Retrofitting of Reinforced Concrete Beam-Column via Steel Jackets against Close-in Detonation. 12th International LS-DYNA Users Conference: Livermore Software Technology Corporation; 2012.
15. Tan SH, Tay SK, Chan R, Chng D. Fluid-Structure Interaction involving Close-in Detonation Effects on Column using LBE MM-ALE Method. 9th European LS-DYNA Conference: DYNAmore GmbH; 2013.
16. Tay SK, Poon JK, Chan R. Modeling Rebar in Reinforced Concrete for ALE Simulations. 14th International LS-DYNA Users Conference: Livermore Software Technology Corporation; 2016.
17. SS EN 1991-1-1: 2008 (2017) Eurocode 1: Actions on structures, Part 1-1: General actions - Densities, self-weight, imposed loads for buildings. Enterprise Singapore; 2017.
18. SS EN 1992-1-1: 2008 Eurocode 2: Design of concrete structures, Part 1-1: General rules and rules for buildings. Enterprise Singapore; 2008.
19. NA SS EN 1992-1-1: 2008 Singapore National Annex to Eurocode 2: Design of concrete structures, Part 1-1: General rules and rules for buildings. Enterprise Singapore; 2008.
20. NA+A1:2017 to SS EN 1991-1-1: 2008 (2017) Eurocode 1: Actions on structures, Part 1-1: General actions - Densities, self-weight, imposed loads for buildings (Incorporating Amendment No.1). Enterprise Singapore; 2017.
21. Manual for the design of concrete building structures to Eurocode 2: Institution of Structural Engineers (IStructE); 2006.
22. SS 560: 2016 Singapore Standard: Specification for steel for the reinforcement of concrete - Weldable reinforcing steel - Bar, coil and decoiled product. Enterprise Singapore; 2016.
23. fib Model Code for Concrete Structures 2010. International Federation for Structural Concrete (fib); 2013.
24. Grassl P. MAT_CDPM (MAT_273) in LS-DYNA [Available from: https://petergrassl.com/Research/DamagePlasticity/CDPMLSDYNA/index.html.
25. Borrvall T, Riedel W. The RHT Concrete Model in LS-DYNA. 8th European LS-DYNA Conference: DYNAmore GmbH; 2011.
26. Schwer L. Strain Rate Induced Strength Enhancement in Concrete: Much ado about Nothing? 7th European LS-DYNA Conference: DYNAmore GmbH; 2009.
27. Magallanes JM, Wu Y, Malvar LJ, Crawford JE. Recent Improvements to Release III of the K&C Concrete Model. 11th International LS-DYNA Users Conference: Livermore Software Technology Corporation; 2010.
28. Crawford JE, Wu Y, Choi H-J, Magallanes JM, Lan S. Use and Validation of the Release III K&C Concrete Material Model in LS-DYNA. 2011. Contract No.: TR-11-36.5.
29. Schwer L. Modeling Pre and Post Tensioned Concrete. 14th International LS-DYNA Users Conference: Livermore Software Technology Corporation; 2016.